

IMAGE PROTECTION FOR ROBUST CROPPING LOCALIZATION AND RECOVERY

Qichao Ying^{1*}, Hang Zhou^{2*}, Xiaoxiao Hu¹, Zhenxing Qian^{1*}, Sheng Li¹ and Xinpeng Zhang¹

¹Fudan University, China, ²Simon Fraser University, Canada.

{qcying20, xxhu20, lisheng, zxqian, zhangxinpeng}@fudan.edu.cn, zhouhang2991@gmail.com

ABSTRACT

Existing image cropping detection schemes ignore that recovering the cropped-out contents can unveil the purpose of the behaved cropping attack. This paper presents **CLR-Net**, a novel image protection scheme addressing the combined challenge of image **C**ropping **L**ocalization and **R**ecovery. We first protect the original image by introducing imperceptible perturbations. Then, typical image post-processing attacks are simulated to erode the protected image. On the recipient's side, we predict the cropping mask and recover the original image. Besides, we propose a novel **F**ine-**G**ained generative **J**PEG simulator (FG-JPEG) as well as a feature alignment network to improve the real-world robustness. Comprehensive experiments prove that the quality of the recovered image and the accuracy of crop localization are both satisfactory.

Index Terms— image protection, image cropping localization, image recovery, robustness

1. INTRODUCTION

Image cropping is the process of removing unwanted areas of an image, which creates focus and strengthens the composition. However, it can also be an extremely cheap and effective way to maliciously alter the underlying meaning. Fig. 1 shows two examples of malicious image cropping forgery. The attackers crop the images and mislead the audience with fake comments. Without the ground truth as a reference, people are easily deceived by what they observe from manipulated images. Existing image cropping detection schemes [1, 2, 3] only predict whether the image is cropped by searching for traces that expose image crops. However, a successful cropping prediction or localization is not enough. To fully investigate the intention of each suspicious cropping behavior, we need to locate the position of the crop in the original image plane, or even recover the original image. In the literature, few schemes [4] are developed for cropping localization and recovery. Moreover, [4] require the images to be untouched and uncompressed so that tiny traces like chromatic aberration and vignetting exist. However, attackers can resize or compress the cropped image to counter that.

* equal contribution. * corresponding author. This work is supported by the National Natural Science Foundation of China under Grants U20B2051.

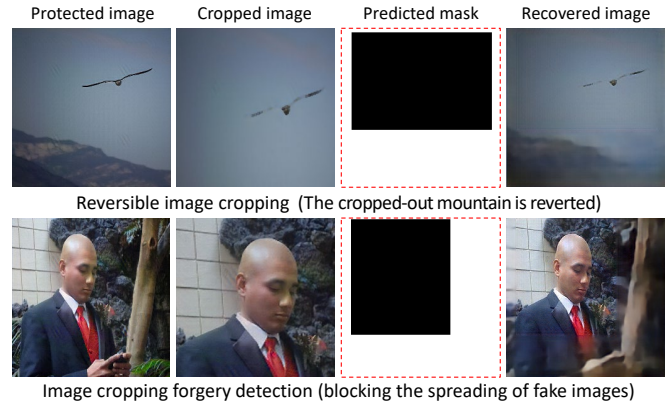


Fig. 1. Application of CLR-Net. We transform images into protected ones via imperceptible signal injection. Once these protected images are cropped, CLR-Net can localize the cropped regions and recovers the cropped-out content.

This paper explores the potential of image protection [5, 6] on image cropping localization and recovery. We first protect the original image by introducing imperceptible perturbations. Then, typical image post-processing attacks are simulated to erode the protected image. On the recipient's side, we predict the cropping mask and recover the original image. For enhanced robustness of CLR-Net in real-world applications, we innovatively propose a novel Fine-Grained generative JPEG simulator (FG-JPEG). Besides, a feature alignment network is proposed to minimize the performance gap against different lossy image operations. Comprehensive experiments demonstrate that CLR-Net accurately estimates the cropping mask and recovers the full image even if the attacker post-processes the cropped image.

It is well notifying that the task of CLR-Net is **Cropped Image Recovery (CIR)** that needs to exactly reconstruct what has been cropped-out by malicious users and predict the cropping mask as well. The goal is different from outpainting that only extend the bordering of a given image using hallucination, i.e., providing non-unique solutions that are visually plausible. CIR is important in many forensics or judicial scenarios that requires exact recovery to see what is cropped-out. In this case, hallucinating possible outcomes using outpainting cannot be accepted.

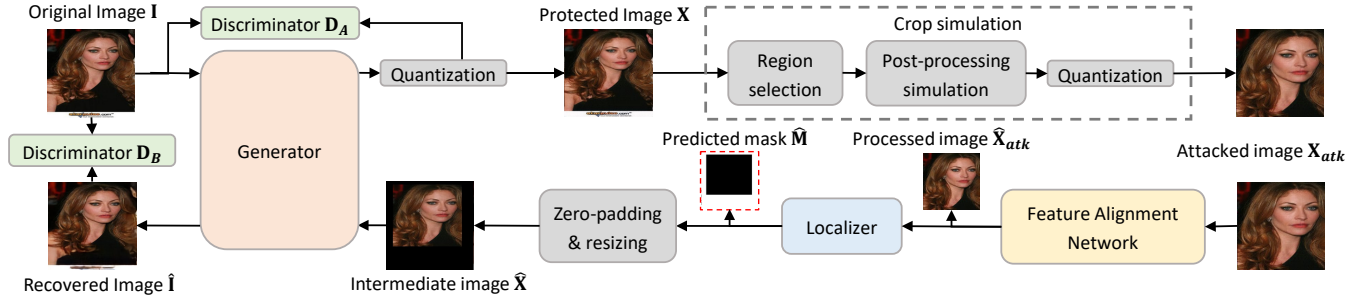


Fig. 2. Approach overview of CLR-Net. The generator transforms the original image into the protected image. The attacked version is then aligned on the recipient’s side, and the localizer predicts the cropping mask. We rectify the processed image by scaling and zero-padding. Finally, the inverse process of the generator estimates the original image.

2. METHOD

2.1. Approach overview

Image Cropping Localization and Recovery (CLR). Cropping and its recovery can be represented by Eq. (1).

$$\begin{aligned} \mathbf{I}_{atk} &= IP(RS(\mathbf{I}, \mathbf{M})), \\ \hat{\mathbf{I}} &= f_{rec}\left(ZR\left(\mathbf{I}_{atk}, \hat{\mathbf{M}}\right)\right), \hat{\mathbf{M}} = f_M(\mathbf{I}_{atk}), \end{aligned} \quad (1)$$

where \mathbf{I} and \mathbf{I}_{atk} denote an image and its attacked version. \mathbf{M} denotes the cropping mask. $RS(\cdot)$ denotes *region selection* that discards the information outside the selected region. $IP(\cdot)$ denotes *image post-processing* that truncates the image and post-processes the rest of the image using lossy operations, e.g., blurring. Our task is respectively to estimate \mathbf{M} and \mathbf{I} given \mathbf{I}_{atk} . We employ two functions $f_M(\cdot)$, $f_{rec}(\cdot)$ respectively for CLR, where $\hat{\mathbf{M}}$ and $\hat{\mathbf{I}}$ are respectively the estimated cropping mask and the recovered image. $ZR(\cdot)$ denotes *zero-padding and resizing* that first zero-pads the attacked image according to the estimated cropping mask and then resizes the padded image into the original size. In most cases, few clues of the cropped-out contents can be found in the rest of the image. So directly solving Eq. (1) will lead to sub-optimal solutions where the destroyed contents are hallucinated rather than truthfully recovered.

Image protection for CLR. To address the above issue, we propose robust image protection for CLR by employing a third function $f_{prt}(\cdot)$ to embed deep representations of an original image, denoted as \mathbf{I} , into itself. Let $\mathbf{X} = f_{prt}(\mathbf{I})$, and we reformulate Eq. (1) as a pair of invertible image embedding and recovery functions, i.e., $\mathbf{X} = f_{prt}(\mathbf{I})$ and $\hat{\mathbf{I}} = f_{rec}\left(ZR\left(\mathbf{X}_{atk}, \hat{\mathbf{M}}\right)\right)$. We expect that $\mathbf{X} \approx \mathbf{I}$, $\hat{\mathbf{I}} \approx \mathbf{I}$ and $\hat{\mathbf{M}} \approx \mathbf{M}$, regardless of the lossy image operations.

The sketch of modeling image cropping and its localization & recovery is presented in Fig. 2. We utilize an attack layer \mathcal{A} to implement *region selection* and *image post-processing* in the real-world application. The localizer \mathcal{L} estimates the cropping mask $\hat{\mathbf{M}}$ and the confidence score S . After

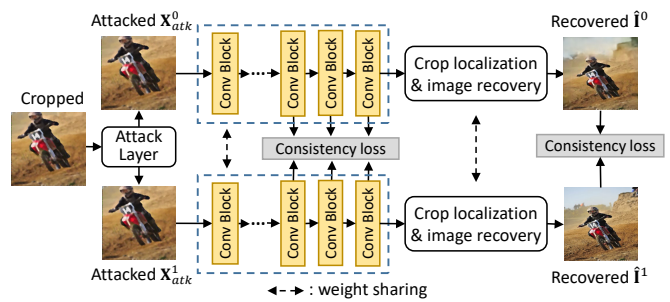


Fig. 3. The Siamese architecture of the feature alignment network. The attack layer generates two attacked views of the cropped image using arbitrarily-sampled attacks. We minimize the consistency loss between the image features as well as the performance gap under the two attacks.

zero-padding and resizing, we send $\hat{\mathbf{X}}$ into the generator \mathcal{G} and inversely run the network to recover \mathbf{I} . We also introduce two discriminators \mathcal{D}_A , \mathcal{D}_B to facilitate the imperceptibility of image protection and the quality of the recovered images.

Mechanisms for enhanced robustness. First, though previous researches have proposed several step-by-step JPEG simulation methods [7, 5], the algorithm and the quantization tables in these schemes are immutable, which is in contrast with real-world compression adaptively controlled by the quality factor and the image content. To address this, we tempt to add more flexibility in JPEG simulation by proposing the novel generative FG-JPEG simulator, as specified in Section 2.2.

Second, $IP(\cdot)$ is likely to contain a large solution space in the real world. Using the attack layer can only provide multi-task guidance, which does not explicitly circumvent uneven network performance against different kinds and strengths of attacks. We introduce a feature alignment network \mathcal{F} to mitigate this issue, as sketched in Fig. 3. In each iteration, we let the attack layer arbitrarily select two kinds of image post-processing attacks and generate two corresponding images \mathbf{X}_{atk}^0 and \mathbf{X}_{atk}^1 from a same \mathbf{X} . On cropping \mathbf{X}_{atk}^0 , \mathbf{X}_{atk}^1 , we use a shared mask \mathbf{M} . Thereafter, \mathcal{F} transforms \mathbf{X}_{atk}^0 , \mathbf{X}_{atk}^1

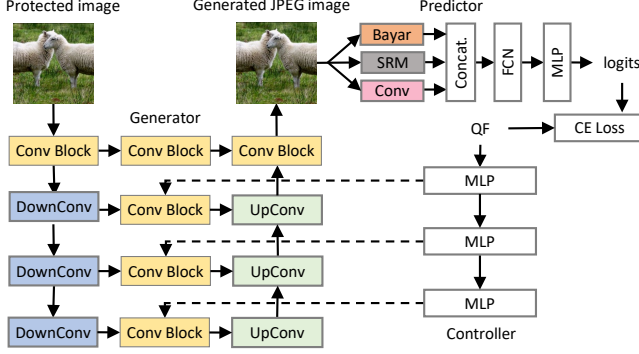


Fig. 4. Network architecture of FG-JPEG. The generator takes the protected image and simulates the JPEG compression, which is conditioned by the controller. The predictor classifies the QF of the generated images.

into $\hat{\mathbf{X}}_{atk}^0, \hat{\mathbf{X}}_{atk}^1$ using the shared parameters. Afterward, we respectively conduct cropping localization and image recovery based on the two views, where the estimated masks, as well as the recovered images, are respectively denoted as $\{\hat{\mathbf{M}}^0, \hat{\mathbf{I}}^0\}, \{\hat{\mathbf{M}}^1, \hat{\mathbf{I}}^1\}$. We restrict that the performance of CLR-Net against the two attacks should be close between each pair, i.e., $\hat{\mathbf{M}}^0 \approx \hat{\mathbf{M}}^1, \hat{\mathbf{I}}^0 \approx \hat{\mathbf{I}}^1$. We also minimize the distance between the representations ϕ_n^0, ϕ_n^1 extracted from $\hat{\mathbf{I}}^0, \hat{\mathbf{I}}^1$. Third, we prevent \mathcal{F} from drastically changing the image, i.e., $\hat{\mathbf{I}}^0 \approx \hat{\mathbf{I}}^1$.

Objective functions. We use the popular ℓ_1 loss term to measure the distance between images.

$$L_{prt} = \|\mathbf{I} - \mathbf{X}\|_1, L_{rec} = \|\mathbf{I} - \hat{\mathbf{I}}\|_1. \quad (2)$$

We minimize the Binary Cross Entropy (BCE) loss between $\hat{\mathbf{M}}$ and \mathbf{M} .

$$\begin{aligned} L_{loc} &= BCE(\mathbf{M}, \hat{\mathbf{M}}) \\ &= -\frac{1}{HW} \sum (\mathbf{M}_{i,j} \log \hat{\mathbf{M}}_{i,j} + (1 - \mathbf{M}_{i,j}) \log (1 - \hat{\mathbf{M}}_{i,j})). \end{aligned} \quad (3)$$

The loss for the two discriminators are respectively shown in Eq.(4), where we accept the most-common BCE loss.

$$\begin{aligned} L_{\mathcal{D}_A} &= -\frac{1}{2}(\log \mathcal{D}_A(\mathbf{I}) + \log (1 - \mathcal{D}_A(\mathbf{X}))), \\ L_{\mathcal{D}_B} &= -\frac{1}{2}(\log \mathcal{D}_A(\mathbf{I}) + \log (1 - \mathcal{D}_A(\hat{\mathbf{I}}))), \\ L_{GAN} &= -(\log \mathcal{D}_A(\mathbf{X}) + \log \mathcal{D}_B(\hat{\mathbf{I}})). \end{aligned} \quad (4)$$

The performance consistency loss for the feature alignment network \mathcal{F} is consist of four loss terms:

$$L_{cs} = \|\hat{\mathbf{M}}^0 - \hat{\mathbf{M}}^1\|_1 + \|\hat{\mathbf{I}}^0 - \hat{\mathbf{I}}^1\|_1 + \|\hat{\mathbf{I}}^0 - \mathbf{I}\|_1 + \sum_{n \in [3,5]} \|\phi_n^0 - \phi_n^1\|_1, \quad (5)$$

where $n \in [3, 5]$ indicates the third to fifth layer of \mathcal{F} .

The total loss for CLR-Net is based on the processed image provided by the student network \mathbf{P}_{stu} .

$$\mathcal{L} = L_{prt} + \alpha \cdot L_{rec} + \beta \cdot L_{loc} + \gamma \cdot L_{cs} + \eta \cdot L_{GAN}. \quad (6)$$

2.2. Network details

To implement \mathcal{G} , we use an invertible U-shaped network [8] composed of three stacked downscaling modules and three upsampling modules. We apply Spectral Normalization (SN) [9] in each block in that SN helps stabilize the training by restricting the Lipschitz constant within one.

For cropping simulation, we freely generate cropping masks \mathbf{M} to crop the protected images. The survival rate is set as $r_c \in [0.5^2, 1^2]$, where 0.5^2 stands for preserving only 25% squared-size area of \mathbf{X} while the rest are cropped. Afterward, we resize the cropped image and simulate common image post-processing attacks using classical differentiable lossy image operations [5]. Lastly, we convert the floating-point values of \mathbf{X} to 8-bit integer to save images on disk.

The feature alignment network \mathcal{F} is sketched in Fig. 3. It is built upon a six-layered fully-convolutional network. Each *Conv* block within the FCN shown in Fig. 3 consists of a *Conv* layer, an ELU activation layer and a SN layer.

FG-JPEG consists of a generator, a controller and a predictor. Fig. 4 illustrates the network design. The predictor classifies the quality factor of a target image, which is implemented by ResNet-32 and trained to estimate the QF of real-world JPEG images \mathbf{I}_{jpg} . We replace the leading *Conv* layer with a vanilla *Conv* layer, an SRM *Conv* layer and a Bayar *Conv* layer in parallel similar to [10] to augment the image details. The generator is built upon the popular four-leveled U-Net architecture, where we introduce an additional *Conv* block to replace the straightforward concatenation in each level. Furthermore, we let the outputs of the lower three levels of the additional *Conv* blocks be conditioned on the output of the controller. The controller is a six-layered MLP, where the last three layers learn the mapping functions that output modulation parameter pairs a, b that control the standard deviation and mean of the outputs.

$$\mathbf{F}_{out,i} = a_i \cdot Conv(\mathbf{F}_{in,i}) + b_i, \quad (7)$$

where \mathbf{F}_{in}^i and \mathbf{F}_{out}^i respectively denote the input and output features of the additional *Conv* block at i_{th} level. The predictor then provides classification results \hat{QF} on $\hat{\mathbf{I}}_{jpg}$, and the results should be close with those of \mathbf{I}_{jpg} with QF . Note that FG-JPEG should be trained ahead of CLR-Net, where we employ the Cross-Entropy (CE) loss.

$$L_{QF} = CE(\mathbf{Q}_o, \mathbf{Q}_r) = -\sum_{c=1}^6 y_{o,c} \log(p_{o,c}), \quad (8)$$

where $y_{o,c}$ is the binary indicator if class label c is the correct classification for observation o . $p_{o,c}$ is the estimated probability observation o is of class c . The QF labels are set as

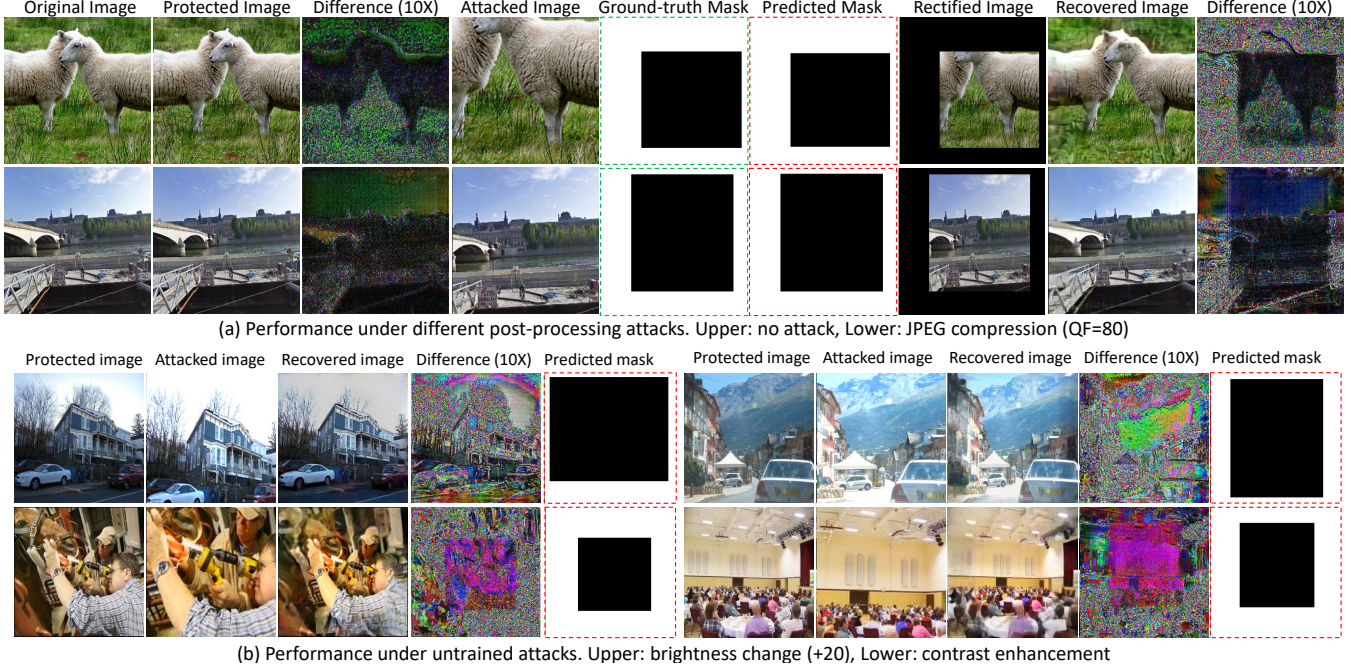


Fig. 5. Qualitative analysis of CLR-Net against different lossy image operations and varied survival rate. The testing image are from COCO, ImageNet and Places.

$QF \in \{10, 30, 50, 70, 90, 100\}$ The JPEG generator and controller are jointly optimized by minimizing:

$$L_{jpg} = \|\mathbf{I}_{jpg} - \hat{\mathbf{I}}_{jpg}\|_1 + \epsilon \cdot CE(QF, \hat{QF}). \quad (9)$$

The localizer \mathcal{L} is built upon a three-layered lightweight U-Net that transforms $\hat{\mathbf{X}}_{atk}$ into a one-dimensional feature. The feature is then flattened and fed into a four-layered MLP. The output of the MLP is $\{x_0, y_0, x_1, y_1, S\}$, where $\{x_0, y_0, x_1, y_1\}$ represents the coordinates of the upper-left and lower-right corner of the rectangle-shaped $\hat{\mathbf{M}}$. \mathbf{X}_{atk} is detected as *cropped* if $S \geq 0.5$. We also feed \mathcal{L} with non-cropped images \mathbf{I} and encourage $S \approx 0$. The two discriminators \mathcal{D}_A and \mathcal{D}_B are built upon the popular Patch-GAN [11].

3. EXPERIMENTS

During training, the original images \mathbf{I} in our scheme are from a mixture of multiple popular image datasets, namely, COCO [12], CelebA [13], Places [14] and ImageNet. We arbitrarily select around 10000 images from the training set of the above datasets. We build the test set in the same way with 1000 images from each. In the following experiments, we resize the images into size 256×256 , and the results under other typical resolutions are close. The hyper-parameters are set as $\alpha = 1.5, \beta = 0.1, \gamma = 0.05, \epsilon = 0.1$ and $\eta = 0.01$. The batch size of CLR-Net during training is set as 4. We use Adam optimizer with the default parameters. The learning rate is 1×10^{-4} with cosine annealing decay.

3.1. Qualitative and quantitative analysis

Quality of the protected images. Fig. 5 showcases four experimental results of CLR-Net on cropping localization and image recovery. We can observe that the quality of \mathbf{X} is satisfactory with the difference between \mathbf{X} and \mathbf{I} almost imperceptible. We have conducted quantitative embedding experiments on different datasets. The averaged PSNR and SSIM between \mathbf{I} and \mathbf{X} is respectively 32.67dB/ 0.933 on COCO, 33.01dB/ 0.937 on ImageNet, and 33.13dB/ 0.940 on Flickr.

Performance of cropping localization and recovery. Fig. 5 further shows the results of cropping localization and image recovery. We can observe that the original images are recovered even with the median blurring attack and a medium-sized cropping mask. The average PSNR between \mathbf{I} and $\hat{\mathbf{I}}$ in these cases is 26.73dB with SSIM 0.843. The cropping localization is accurate, with the average F1 score close to 0.95. We have conducted more experiments over the test set under different survival rate and benign attacks. The average performances are reported in Table 1. For image recovery, the average SSIMs are generally above 0.8, which can provide satisfying and trustworthy recovery results. Table 1 also reports quantitative results on untrained attacks, where the performance gaps between trained and untrained attacks are acceptable.

3.2. Comparisons

Image recovery from the cropped version. There is no previous work that recovers the entire image from its cropped

Table 1. Average performance of cropping localization and image recovery over 1000 images from different datasets.

Survival rate	Dataset	Index	JPEG			Scaling			M-Blur	CE	Dropout	Identity
			QF90	QF70	QF50	150%	125%	75%				
[0.5 ² ,0.65 ²]	CelebA	F1	0.955	0.940	0.921	0.956	0.933	0.947	0.935	0.827	0.864	0.980
		PSNR	26.50	24.55	23.40	25.74	25.46	26.13	26.61	22.47	23.39	27.77
		SSIM	0.790	0.753	0.719	0.797	0.770	0.814	0.816	0.701	0.710	0.829
[0.65 ² ,0.8 ²]	COCO	F1	0.968	0.970	0.951	0.963	0.970	0.956	0.941	0.912	0.920	0.986
		PSNR	27.46	27.30	22.20	26.34	24.94	25.75	26.34	23.04	25.46	30.18
		SSIM	0.866	0.854	0.707	0.801	0.767	0.769	0.755	0.731	0.789	0.891
[0.8 ² ,1.0 ²]	Places	F1	0.982	0.979	0.965	0.970	0.958	0.969	0.947	0.901	0.885	0.990
		PSNR	29.70	27.55	25.92	27.69	27.62	29.29	26.80	26.62	22.09	31.07
		SSIM	0.844	0.819	0.774	0.853	0.846	0.849	0.811	0.772	0.740	0.898



Fig. 6. Comparison of cropped image recovery with [6] and outpainting, a related technology. Owing to more sophisticated and targeted design of network bias and FG-JPEG, our proposed method surpasses [6] noticeably.

version. In Table 1, we compare our method with [6] by extending it from manipulated content recovery to image cropping recovery. We find that though the method can somehow localize the cropped region well, the performance of [6] concerning cropping recovery has a noticeable gap compared to ours. Besides, we further compare the method with Stable Diffusion-Infinity¹, which is typically designed for outpainting. We find that though the network can produce extra-high-quality results with astonishing details and imagination, yet the outpainted contents cannot ensure fidelity with reference to the original ones. In contrast, CLR-Net pursues the “exactness” of cropped content recovery, which emphasizes more on fidelity rather than “feasibility”.

Cropping identification and localization. The overall accuracy of Van et al. [4] is 86% on uncompressed images. Whenever the input images are compressed or tainted by other

¹<https://huggingface.co/spaces/Inyan/stablediffusion-infinity>

Table 2. Quantitative performance comparison between our method (CLR-Net, 1000 images), Imuge [6] (1000 images) and outpainting (Stable Diffusion, 100 images). For [6], we control that the PSNR before and after image protection should be around 33dB for fair comparison.

Method	NoAtk		JPEG70		Scaling		M-Blur	
	F1	PSNR	F1	PSNR	F1	PSNR	F1	PSNR
Imuge [B]	.944	26.55	.909	23.97	.922	25.48	.885	24.15
Stable Diffusion	-	17.42	-	17.63	-	-	-	-
Ours (CLR-Net)	.986	30.18	.970	27.30	.963	26.34	.947	26.80

digital attacks, the scheme can no longer predict the cropping mask. The cropping prediction accuracy of CLR-Net is 95.41% that further leads by a large margin. Note that in the result we include the false alarm rate where we should not predict *positive* on non-cropped images.

3.3. Ablation studies

Influence of feature alignment and FG-JPEG. We see a promising performance gain by the feature alignment operation. It proves that the network can help unify I_{atk} made by different benign attacks, and therefore allow the generator to work on a more clustered transformed domain. From Fig. 7 and Table 3, the PSNR results suggest that our generative method gives closer results to the real-world JPEG images. The averaged QF classification accuracy of Diff-JPEG [7] is 72.48%, while that of FG-JPEG is 93.17%. It indicates that more knowledge about JPEG compression is learned by FG-JPEG with the joint guidance of the generative model and the QF predictor. Besides, the chess-board artifact of JPEG compression can also be found in the generated JPEG images.

Influence of INN architecture. A typical alternative is to model image protection and image recovery independently using the traditional *encoder-decoder* networks. Thus, we implement the image protection network and the image recovery network using two simple U-Nets. For a fair comparison, we regulate that the two networks contain the same number of parameters in sum with CLR-Net. From Table 4, we observe that INN-based CLR-Net provides better performance.

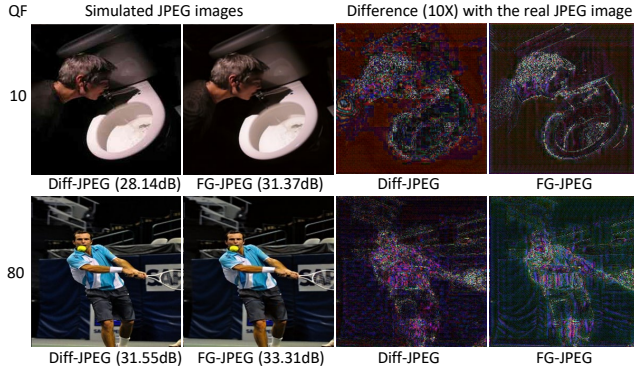


Fig. 7. Comparison on the fidelity of the simulated JPEG images between FG-JPEG and Diff-JPEG [7].

Table 3. Comparison of different JPEG simulators by measuring the average PSNR between the ground-truth and simulated JPEG images (QF=70).

	FG-JPEG	Diff-JPEG	JPEG-Mask	JPEG-SS
PSNR	32.55	31.42	28.49	30.77
Accuracy	93.17%	72.48%	64.55%	73.42%

Table 4. Averaged results of ablation studies on COCO. The tests are done under JPEG attack (QF=70) and $r_c = 0.7^2$.

Setting	F1	PSNR	SSIM
w/o feature alignment ($\hat{\mathbf{X}}_{atk} = \mathbf{X}_{atk}$)	0.958	24.12	0.736
separate \mathbf{G} using two U-Nets	0.933	21.54	0.713
\mathbf{A} using Diff-JPEG [7]	0.958	25.95	0.814
CLR-Net (Full implementation)	0.965	27.02	0.822

4. CONCLUSION

This paper proposes an image protection scheme for image cropping localization and recovery. We formulate a model of the problem upon an INN-based anti-crop generator as well as a crop localizer. Comprehensive experiments prove the effectiveness of CLR-Net.

5. REFERENCES

- [1] Marco Fanfani, Massimo Iuliani, Fabio Bellavia, Carlo Colombo, and Alessandro Piva, “A vision-based fully automated approach to robust image cropping detection,” *Signal Processing: Image Communication*, vol. 80, pp. 115629, 2020.
- [2] Ido Yerushalmy and Hagit Hel-Or, “Digital image forgery detection based on lens and sensor aberration,” *International Journal of Computer Vision*, vol. 92, no. 1, pp. 71–91, 2011.
- [3] Weihai Li, Yuan Yuan, and Nenghai Yu, “Passive detection of doctored jpeg image via block artifact grid extraction,” *Signal Processing*, vol. 89, no. 9, pp. 1821–1829, 2009.
- [4] Basile Van Hoorick and Carl Vondrick, “Dissecting image crops,” in *Proceedings of the IEEE/CVF International Conference on Computer Vision*, 2021, pp. 9741–9750.
- [5] Jiren Zhu, Russell Kaplan, Justin Johnson, and Li Fei-Fei, “Hidden: Hiding data with deep networks,” in *Proceedings of the European Conference on Computer Vision (ECCV)*, 2018, pp. 657–672.
- [6] Qichao Ying, Zhenxing Qian, Hang Zhou, Haisheng Xu, Xinpeng Zhang, and Siyi Li, “From image to imuge: Immunized image generation,” in *Proceedings of the 29th ACM international conference on Multimedia*, 2021, pp. 1–9.
- [7] Richard Shin and Dawn Song, “Jpeg-resistant adversarial images,” in *NIPS 2017 Workshop on Machine Learning and Computer Security*, 2017, vol. 1.
- [8] Mingqing Xiao, Shuxin Zheng, Chang Liu, Yaolong Wang, Di He, Guolin Ke, Jiang Bian, Zhouchen Lin, and Tie-Yan Liu, “Invertible image rescaling,” in *European Conference on Computer Vision*. Springer, 2020, pp. 126–144.
- [9] Takeru Miyato, Toshiki Kataoka, Masanori Koyama, and Yuichi Yoshida, “Spectral normalization for generative adversarial networks,” *arXiv preprint arXiv:1802.05957*, 2018.
- [10] Yue Wu, Wael AbdAlmageed, and Premkumar Natarajan, “Mantra-net: Manipulation tracing network for detection and localization of image forgeries with anomalous features,” in *Proceedings of the IEEE/CVF Conference on Computer Vision and Pattern Recognition*, 2019, pp. 9543–9552.
- [11] Phillip Isola, Jun-Yan Zhu, Tinghui Zhou, and Alexei A Efros, “Image-to-image translation with conditional adversarial networks,” in *Proceedings of the IEEE Conference on Computer Vision and Pattern Recognition*, 2017, pp. 1125–1134.
- [12] Tsung-Yi Lin, Michael Maire, Serge Belongie, James Hays, Pietro Perona, Deva Ramanan, Piotr Dollár, and C Lawrence Zitnick, “Microsoft coco: Common objects in context,” in *European Conference on Computer Vision*. Springer, 2014, pp. 740–755.
- [13] Ziwei Liu, Ping Luo, Xiaogang Wang, and Xiaoou Tang, “Large-scale celebfaces attributes (celeba) dataset,” *Retrieved August*, vol. 15, no. 2018, pp. 11, 2018.
- [14] Bolei Zhou, Agata Lapedriza, Aditya Khosla, Aude Oliva, and Antonio Torralba, “Places: A 10 million image database for scene recognition,” *IEEE transactions on pattern analysis and machine intelligence*, vol. 40, no. 6, pp. 1452–1464, 2017.